ChemComm

The Contrasting Impacts of Polyethylene Glycol on Electrochemical Behaviors of Fe and Zn Metal Anodes in Aqueous Batteries

Journal:	*ChemComm*
Manuscript ID	CC-COM-03-2025-001196.R1
Article Type:	Communication

ChemComm

COMMUNICATION

The Contrasting Impacts of Polyethylene Glycol on Electrochemical Behaviors of Fe and Zn Metal Anodes in Aqueous Batteries

Received 00th January 20xx,
Accepted 00th January 20xx

DOI: 10.1039/x0xx00000x

Sungjin Yang,[a†] Cheng Chen,[a†], Xingyi Lyu,[b] Soenke Seifert,[c] Hunter Maclennan,[a] Min Soo Jung,[a] Emmanuel Nyela Musa,[a] Yiming Sui,[a] Alexis M. Scida,[a] Riitvek Baddireddi,[a] Maxine A. McNerney,[a] Kyriakos Stylianou,[a] Tao Li,*[b,c] Chong Fang, *[a] and Xiulei Ji*[a]

Polyethylene glycol (PEG) is considered an electrolyte additive to improve the performance of aqueous batteries. Here, we report that PEG enhances the Coulombic efficiency (CE) of an Fe metal anode (FeMA) in aqueous $FeCl_2$ electrolytes but surprisingly lowers the CE of Zn metal anode (ZMA) in concentrated $ZnCl_2$ electrolytes. We observed that the PEG addition raises the corrosion potential of FeMA but decreases that for ZMA. The femtosecond stimulated Raman spectroscopy (FSRS) and synchrotron small-angle X-ray scattering (SAXS) results reveal that PEG solvates Fe^{2+} rather than Zn^{2+} in the chloride-rich environments.

Transitioning from fossil fuels to renewable energy sources necessitates the installation of grid energy storage to levelize intermittent power generation cycles.[1,2] For storage batteries, energy density is no longer the foremost concern. This opens the door to alternative devices, including aqueous metal batteries, which are promising due to their attributes of greater safety, low cost, and smaller environmental impacts.[3–5] Among these batteries, Zn metal batteries (ZMBs) have received much attention and are poised for commercial applications in the near future,[4] and Fe-ion batteries (FeIBs) are seeing increasing efforts, relishing the ultimate sustainability of iron metal and its minimal cost.[6] However, the cycle life of these aqueous metal batteries is often challenged by the limited reversibility of their metal anodes. The primary contributor to their irreversibility is the hydrogen evolution reaction (HER), a parasitic reaction between metal anodes as a reductant and water in aqueous electrolytes as an oxidant, resulting in a low Coulombic efficiency (CE) during the plating-stripping cycles.[7]

To mitigate HER, various strategies have been proposed. Kinetically, the corrosion of metal anodes can be slowed down by growing a solid electrolyte interphase (SEI) layer that passivates the metal surface.[8,9] Thermodynamically, different lattice planes of metal anodes can exhibit varying corrosion resistance, and plating a more stable lattice can be induced epitaxially.[10,11] In addition, HER relates to the solvation structures of electrolytes, and highly concentrated electrolytes have delivered enhanced performance.[12] On the other hand, electrolyte additives are known capable of modulating the solvation structures of electrolytes. Polyethylene glycol (PEG) is cost-effective and environmentally friendly, making it a practical choice of additive/co-solvent. Pioneering studies have demonstrated that PEG added to the aqueous electrolytes can effectively suppress HER and promote uniform plating of the Zn metal anode (ZMA).[13,14] However, it remains elusive how the PEG interacts with Zn^{2+} and Fe^{2+}, comparatively, in the presence of high concentrations of chlorides, regarding the impacts on the reversibility of their metal anodes.

Herein, we investigate the impacts of PEG 200—where 200 denotes its average molar mass—on the performance of $FeCl_2$ and $ZnCl_2$ electrolytes, where PEG 200 is miscible with these electrolytes due to its relatively low molar mass. We report that adding PEG causes the opposite effects: improving the CE for the Fe metal anode (FeMA) but lowering the CE of the ZMA in their concentrated chloride electrolytes. Interestingly, the addition of PEG shifts the corrosion potentials of FeMA and ZMA in opposite directions: higher for the FeMA, but lower for the ZMA. This disparity was elucidated by our results of the structure-sensitive ground-state femtosecond stimulated Raman spectroscopy (GS-FSRS) and synchrotron small-angle X-ray scattering (SAXS), which revealed that PEG

[a] Department of Chemistry, Oregon State University Corvallis, Oregon 97331-4003, USA. Email: David.Ji@oregonstate.edu, Chong.Fang@oregonstate.edu
[b] Department of Chemistry and Biochemistry, Northen Illinois University, DeKalb, Illinois 60115, USA.
[c] X-ray Science Division, Argonne National Laboratory, Lemont, Illinois 60439, USA. Email: tli4@niu.edu
† These authors contributed equally.
Supplementary Information available: [details of any supplementary information available should be included here]. See DOI: 10.1039/x0xx00000x

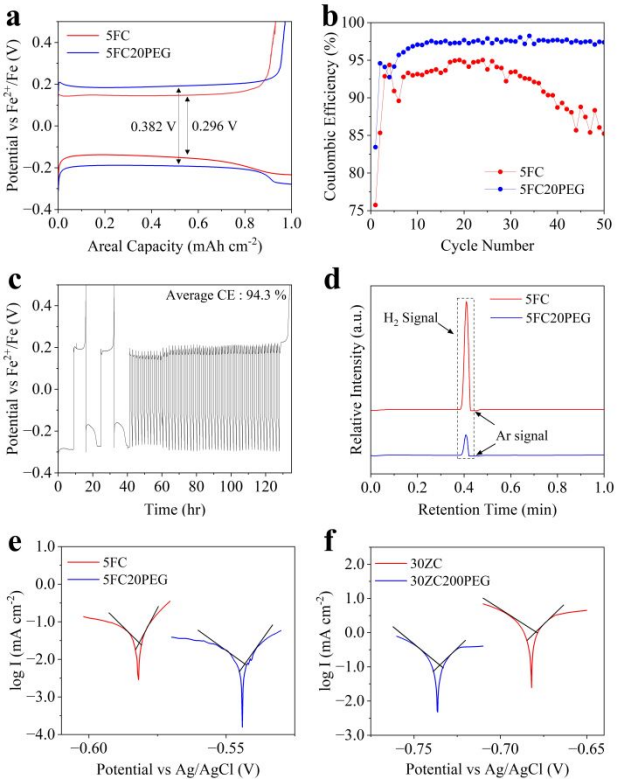

Fig. 1. The electrochemical performance of the FeMA at a current density of 1 mA cm^{-2}, with each plating and stripping process lasting for 1 hour. (a) GCD profiles of the 10th cycle. (b) CE tests for 5FC and 5FC20PEG. (c) GCD profiles for 5FC20PEG to determine the average CE at a current density of 1 mA cm^{-2}. (d) GC profiles with an argon carrier gas. Tafel plots of three-electrode Swagelok cells with an Ag/AgCl reference electrode, scanned at 10 mV min^{-1}: (e) Fe foil (500 µm) serves as both the working and counter electrode. (f) Zn foil (250 µm) as both the working and counter electrode.

chains are able to solvate Fe^{2+} but not Zn^{2+}. With additional tests of other transition metal-ion electrolytes, it is evident that the ability of the metal salts to form chloro-complexes regulates interactions between PEG molecules and transition metal-ions, thus their resulting changes of electrochemical reversibility upon adding PEG.

First, we evaluated the reversibility of FeMA in different concentrations of aqueous $FeCl_2$. We found that 5 *m* $FeCl_2$ delivers a superior CE to 1, 2, 3, and 4 *m* over 50 cycles (Fig. S1a), and concentrations beyond 5 *m* $FeCl_2$ approach the solubility limit, thus not being considered. Galvanostatic charge-discharge (GCD) potential profiles reveal that the overpotential decreases as concentration increases until 3 *m* (Fig. S1b). We selected 5 *m* $FeCl_2$ as the base electrolyte (5FC) and screened the CE by varying the amounts of PEG added to this electrolyte. We prepared electrolytes with 0, 5, 10, 20, 50, and 100 wt% PEG added, denoted as 5FC, 5FC5PEG, 5FC10PEG, 5FC20PEG, 5FC50PEG, and 5FC100PEG, respectively. Herein, the wt% of PEG refers to the mass ratio of PEG versus all water in the electrolytes, including that from the hydrated salt.

The GCD profiles of these electrolytes reveal the optimal CE of iron plating and stripping for 5FC20PEG (Fig. S2). However, compared to 5FC, 5FC20PEG exhibited a greater extent of potential hysteresis from 0.296 V and 0.382 V (Fig. 1a). This suggests sluggish diffusion of Fe^{2+} ions when PEG is present, as evidenced by the comparison of the R_s values for both electrolytes (Fig. S3).[15] Despite the increased potential hysteresis, 5FC20PEG exhibits a higher CE than 5FC, from 75.7% to 83.4% initially, and from 93.2% to 97.5% after 10 cycles (Fig. 1b). To assess the reversibility of the FeMA, we also measured the average CE with the reservoir method,[6] where the CE increases 92.9% for 5FC (Fig. S4) to 94.3% for 5FC20PEG under the same conditions (Fig. 1c). Overpotential increases during the individual plating process may relate to the increasing nucleation activation energy during the progressive plating process. This means the plated iron surface renders the following iron plating more difficult (Fig. S5). We performed the gas chromatography (GC) analysis during the plating and stripping processes, and the results showed that 5FC produced 3.0 µmol of H_2, in contrast to only 0.40 µmol for 5FC20PEG (Fig. 1d). These findings clearly indicate that the addition of PEG suppresses the HER from FeMA, enhancing its performance.[16]

We also measured the average CE with varying amounts of PEG in 30 *m* $ZnCl_2$: 0, 50, 100, and 200 wt% versus water in the electrolytes (designated as 30ZC, 30ZC50PEG, 30ZC100PEG, and 30ZC200PEG, respectively), following the reservoir method, reported by Hoang *et al*.[17] Unfortunately, the results indicate that as the concentration of PEG increases, the CE decreased, from 98.0% in 30ZC to 96.4% in 30ZC200PEG (Fig. S6). Interestingly, during cycling, the 30ZC200PEG electrolyte still produced less hydrogen gas, 0.057 µmol, compared to the 30ZC electrolyte, which generated 0.46 µmol (Fig. S7). This suggests that HER suppression does not always correspond to improved reversibility of the transition metal anode.

We collected the Tafel plots for FeMA and ZMA in their respective electrolytes and found that the exchange current density decreases for both metal anodes with the addition of PEG. Evidently, PEG slows down the plating/stripping kinetics by increasing the electrolyte viscosity.[18] Nevertheless, the changes of the corrosion potential display the opposite trends for the two metals. For the FeMA, the corrosion potential increases from –0.58 V of 5FC to –0.54 V of 5FC20PEG; as for ZMA, the corrosion potential decreases from –0.68 V of 30ZC to –0.74 V of 30ZC200PEG (Fig. 1e and f). Thus, FeMA and ZMA become more and less stable, respectively, with PEG added, consistent with the CE results.

We consider that the corrosion potential is affected by the solvation structures of the metal ions to be plated.[19–21] We employed the GS-FSRS to study $FeCl_2$ electrolytes with varying amounts of PEG. The peak at ~355 cm^{-1} of the FSRS spectra is attributed to the solvated ferrous ion, i.e., $[Fe(OH_2)_6]^{2+}$ initially.[22] As the amount of PEG increases, this peak redshifts with much higher intensity, indicating the altered coordination environment of Fe^{2+} ions with PEG participating in the solvation shells of Fe^{2+}. The postulation is supported by FSRS spectrum of 1 *m* $FeCl_2$ dissolved in pure PEG (Fig. 2a). Note that this

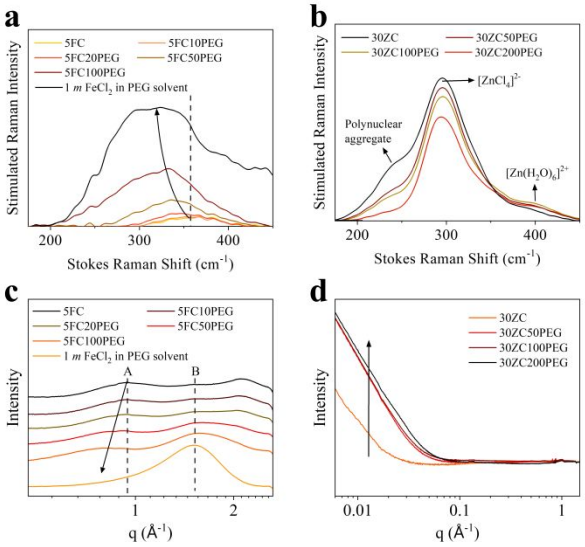

Fig. 2. FSRS spectra for (a) $FeCl_2$ and (b) $ZnCl_2$ electrolytes with varying amounts of PEG added. SAXS spectra for (c) $FeCl_2$ and (d) $ZnCl_2$ electrolytes with varying amounts of PEG added.

$FeCl_2$/PEG solution appears light yellow rather than light green of aqueous counterparts (Fig. S9).[23] For the $ZnCl_2$ electrolytes, the FSRS spectra exhibit no significant peak shift with increasing amounts of PEG. The peaks at ~295 and 395 cm^{-1}, corresponding to the $[ZnCl_4]^{2-}$ and $[Zn(OH_2)_6]^{2+}$ complex ions, respectively, do not exhibit noticeable shifts.[24] Such results suggest that PEG cannot replace either chloride or water in the first coordination shells of Zn^{2+}. Additionally, we observed that the peak at ~240 cm^{-1}, associated with Zn-Cl polynuclear aggregates, gradually diminishes as the PEG concentration increases (Fig. 2b).[25] This suggests the dilution effect of PEG, where the PEG chains help divide the large Zn-Cl polynuclear aggregates into smaller ones but still cannot penetrate to the first coordination shell. Therefore, if the additives do not interact with transition metal ions directly, the corrosion potential tends to decrease due to the shear concentration reduction, as the additives dilute the electrolyte, according to the Nernst equation.[20] This is the case of PEG added to the 30 *m* $ZnCl_2$ electrolytes. However, for the case of PEG in the Fe^{2+} electrolytes, the PEG chains manage to replace some aqua ligands of $[Fe(OH_2)_6]^{2+}$.[21] Since the interactions between the solvating PEG and Fe^{2+} ions are spatially frustrated, the desolvation energy penalty for Fe^{2+} ions originated from cleaving the bonds with PEG is reduced.[26] This explains why the corrosion potential tends to increase despite the decrease of concentration of Fe^{2+} for the $FeCl_2$ electrolytes.[27]

Small angle X-ray scattering (SAXS) has been widely used to study the solvation structures.[28] As shown in Fig. 2c, the peak A's position is approximately 0.9 $Å^{-1}$ for 5FC in water, corresponding to a real space $d_{spacing}$ of about 6.9 Å ($d_{spacing}$ =2π/q).[29] This distance agrees with the diameter of the cluster of $[Fe(OH_2)_6]^{2+}$ complex. Upon the addition of PEG, peak A shifts toward the low q region, which suggests an increase in the size of the solvated ferrous ion. This size increase indicates a transformation of $[Fe(OH_2)_6]^{2+}$ to a larger Fe^{2+} complex with PEG in the solvation shell, partially replacing aqua ligand. This result is in agreement with the FSRS data and electrochemical performance. In addition, there is a weak peak located around 1.5 $Å^{-1}$ in 5FC, which corresponds to the $d_{spacing}$ of about 4.2 Å and can be attributed to the distance between two oxygen atoms of $[Fe(OH_2)_6]^{2+}$. However, in the 5FC with PEG/H2O mixed solvent, the peak B comes not only from the oxygen correlation within the cluster, but also from the PEG solvent itself (Fig. S10). For the ZC samples, no such peaks can be observed in the middle q to high q region. The only difference that can be observed is from the low q region. With the addition of PEG, large aggregates (larger than 200 nm) could be predicted from the profiles.

We posit that the formation of halide-complex ions by Zn^{2+} hinders the interactions of Zn-ions with PEG. To test this hypothesis, we analyzed Tafel plots of 2 *m* $Zn(OTf)_2$ and 5 *m* $ZnBr_2$ electrolytes, before and after adding 200 wt% PEG, referred to as 2ZO, 2ZO200PEG, 5ZB, and 5ZB200PEG. In sharp contrast, the corrosion potential of ZMA increases from –0.82 V to –0.80 V with 200 wt% PEG in 2 *m* $Zn(OTf)_2$ (Fig. S11a), whereas, the corrosion potential of ZMA decreases from –0.86 V to –0.91 V after 200 wt% PEG was added in 5 *m* $ZnBr_2$ (Fig. S11b). Note that $ZnBr_2$ forms metal halide complexes,[30] while $Zn(OTf)_2$ does not. In both electrolytes, the exchange current density decreases upon the addition of PEG.

We also investigated other transition metal chloride electrolytes, including 5 *m* $CuCl_2$ and 5 *m* $MnCl_2$ electrolytes, with the addition of 200 wt% PEG, denoted as 5CC, 5CC200PEG, 5MC, and 5MC200PEG, which exhibited similar disparities (Table. S1). [31,32] To understand these differences, we considered why they behave differently, regarding their coordination environments (See more explanation and Table S2 in ESI). With the addition of 200 wt% PEG, the corrosion potential of Cu metal decreased from 0.23 V to 0.083 V in the PEG-diluted $CuCl_2$ electrolyte (Fig. S11c), while in the $MnCl_2$ electrolyte, adding 200 wt% PEG caused the corrosion potential to increase from –1.13 V to –1.07 V (Fig. S11d). The exchange current density decreased in both electrolytes as well. We also observed HER bubbling off the Mn free-standing film (Fig. S12), which may explain the fluctuations observed in the Tafel plots of Mn metal anode (Fig. S11d).[33]

In summary, our study shows that addition of PEG enhances the reversibility of FeMA in an $FeCl_2$ electrolyte but compromises that of ZMA in a concentrated $ZnCl_2$ electrolyte. According to the Tafel plots, the addition of PEG raises the corrosion potential for FeMA but decreases that for ZMA. The disparity stems from the ability or inability of the transition metal ions to form their halide complex ions, which regulates whether metal-ions are allowed to interact with PEG chains. When such metal-halide complex ions are formed, such as in $ZnCl_2$, PEG merely serves as a dilute rather than a solvent, causing a decrease in corrosion potential and the compromised reversibility with its addition. Conversely, when the electrolyte cannot form these complex ions, as in $FeCl_2$, PEG interacts

directly with the transition metal ions, reduces the desolvation penalty, and increases the corrosion potential, thereby benefiting the reversibility of the metal electrodes. The results offer valuable insights to promote the applications of aqueous metal batteries.

The authors are grateful to the U.S. National Science Foundation (NSF) for the financial support with the Awards, CHE 2433821, DMR 2221645 and Grant No.2120559, 2342334, and 2323117. This work is supported by the Aqueous Battery Consortium, an energy innovation hub under the US Department of Energy, Office of Basic Energy Sciences, Division of Materials Science and Engineering.

Conflicts of interest

There are no conflicts to declare.

Author Contributions

X.J. concept; S. Y. investigation lead; C. C. and C. F. Raman; X. L., S. S. and T. L. SAXS; H. M., M. A. M. experiments; M. S. J., E. N. M., Y. S., A. M. S., R. B., K. S. other characterization. All authors contribute to the writing of this manuscript.

Data Availability Statement

The data supporting this article have been included as part of the Supplementary Information.

Notes and references

1 H. Hou, W. Lu, B. Liu, Z. Hassanein, H. Mahmood and S. Khalid, *Sustain.*, 2023, **15**, 2048.

2 T. M. Gür, *Energy Environ. Sci.*, 2018, **11**, 2696–2767.

3 M. D. Slater, D. Kim, E. Lee and C. S. Johnson, *Adv. Funct. Mater.*, 2013, **23**, 947–958.

4 S. Zhu, Q. Wang and J. Ni, *EnergyChem*, 2023, **5**, 100097.

5 S. Bi, S. Wang, F. Yue, Z. Tie and Z. Niu, *Nat. Commun.*, 2021, **12**, 6991.

6 X. Wu, A. Markir, Y. Xu, C. Zhang, D. P. Leonard, W. Shin and X. Ji, *Adv. Funct. Mater.*, 2019, **29**, 1900911.

7 Q. Nian, X. Zhang, Y. Feng, S. Liu, T. Sun, S. Zheng, X. Ren, Z. Tao, D. Zhang and J. Chen, *ACS Energy Lett.*, 2021, **6**, 2174–2180.

8 D. Li, L. Cao, T. Deng, S. Liu and C. Wang, *Angew. Chem. Int. Ed.*, 2021, **60**, 13035–13041.

9 H. Jiang, L. Tang, Y. Fu, S. Wang, S. K. Sandstrom, A. M. Scida, G. Li, D. Hoang, J. J. Hong, N. C. Chiu, K. C. Stylianou, W. F. Stickle, D. Wang, J. Li, P. A. Greaney, C. Fang and X. Ji, *Nat. Sustain.*, 2023, **6**, 806–815.

10 J. Zheng, Q. Zhao, T. Tang, J. Yin, C. D. Quilty, G. D. Renderos, X. Liu, Y. Deng, L. Wang, D. C. Bock, C. Jaye, D. Zhang, E. S. Takeuchi, K. J. Takeuchi, A. C. Marschilok and L. A. Archer, *Science*, 2019, **366**, 645–648.

11 H. Liu, Z. Zhu, Q. Yan, S. Yu, X. He, Y. Chen, R. Zhang, L. Ma, T. Liu, M. Li, R. Lin, Y. Chen, Y. Li, X. Xing, Y. Choi, L. Gao, H. S. yun Cho, K. An, J. Feng, R. Kostecki, K. Amine, T. Wu, J. Lu, H. L. Xin, S. P. Ong and P. Liu, *Nature*, 2020, **585**, 63–67.

12 A. Bayaguud, Y. Fu and C. Zhu, *J. Energy Chem.*, 2022, **64**, 246–262.

13 J. Xie, Z. Liang and Y. C. Lu, *Nat. Mater.*, 2020, **19**, 1006–1011.

14 Z. Cao, X. Zhu, S. Gao, D. Xu, Z. Wang, Z. Ye, L. Wang, B. Chen, L. Li, M. Ye and J. Shen, *Small*, 2022, **18**, 2103345.

15 Y. Jin, K. S. Han, Y. Shao, M. L. Sushko, J. Xiao, H. Pan and J. Liu, *Adv. Funct. Mater.*, 2020, **30**, 2003932.

16 L. C. Greenburg, J. Holoubek, Y. Cui, P. Zhang, H. Ai, E. Zhang, C. Liu, G. Feng and Y. Cui, *ACS Energy Lett.*, 2025, **10**, 1022–1029.

17 D. Hoang, Y. Li, M. S. Jung, S. K. Sandstrom, A. M. Scida, H. Jiang, T. C. Gallagher, B. A. Pollard, R. Jensen, N. C. Chiu, K. Stylianou, W. F. Stickle, P. A. Greaney and X. Ji, *Adv. Energy Mater.*, 2023, **13**, 2301712.

18 M. C. M. Sequeira, H. M. N. T. Avelino, F. J. P. Caetano and J. M. N. A. Fareleira, *J. Chem. Eng. Data*, 2023, **68**, 64–72.

19 M. Pourbaix, *J. Electrochem. Soc.*, 1954, **101**, 217C.

20 G. T. Burstein and R. J. Cinderey, *Corros. Sci.*, 1992, **33**, 475–492.

21 C. Huang, X. Zhao, Y. Hao, Y. Yang, Y. Qian, G. Chang, Y. Zhang, Q. Tang, A. Hu and X. Chen, *Energy Environ. Sci.*, 2023, **16**, 1721–1731.

22 H. Kanno and J. Hiraishi, *J. Raman Spectrosc.*, 1982, **12**, 224–227.

23 J. Chen, S. K. Spear, J. G. Huddleston and R. D. Rogers, *Green Chem.*, 2005, **7**, 64–82.

24 D. E. Irish, B. Mccarroll and T. F. Young, *J. Chem. Phys.*, 1963, **39**, 3436–3444.

25 C. Zhang, J. Holoubek, X. Wu, A. Daniyar, L. Zhu, C. Chen, D. P. Leonard, I. A. Rodríguez-Pérez, J. X. Jiang, C. Fang and X. Ji, *Chem. Comm.*, 2018, **54**, 14097–14099.

26 C. W. Kim, J. T. Someren, M. Kirshen and C. Rha, *Phys. Chem. Liq.*, 1988, **18**, 11–20.

27 H. Jin, S. Dai, K. Xie, Y. Luo, K. Liu, Z. Zhu, L. Huang, L. Huang and J. Zhou, *Small*, 2022, **18**, 2106441.

28 X. Liu, L. Fang, X. Lyu, R. E. Winans and T. Li, *Chem. Mater.*, 2023, **35**, 9821–9832.

29 X. Lyu, H. Wang, X. Liu, L. He, C. Do, S. Seifert, R. E. Winans, L. Cheng and T. Li, *ACS Nano*, 2024, **18**, 7037–7045.

30 T. Takamuku, M. Ihara, T. Yamaguchi and H. Wakita, *Z. Naturforsch.*, 1992, **47**, 485–492.

31 H. B. Yi, F. F. Xia, Q. Zhou and D. Zeng, *J. Phys. Chem. A*, 2011, **115**, 4416–4426.

32 C. H. Gammons and T. M. Seward, *Geochim. Cosmochim. Acta*, 1996, **60**, 4295–4311.

33 M. Wang, Y. Meng, Y. Xu, D. Shen, P. Tong and W. Chen, *ACS Energy Lett.*, 2024, **9**, 1381–1388.

Data Availability Statement

The data supporting this article have been included as part of the Supplementary Information.